Обзор ArXiv/astro-ph, 9-14 декабря 2022

От Сильченко О.К.

ArXiv: 2212.05070

DESI Survey Validation Spectra Reveal an Increasing Fraction of Recently Quenched Galaxies at $z \sim 1$

David J. Setton,[1] Biprateep Dey,[1] Gourav Khullar,[1] Rachel Bezanson,[1] Jeffrey A. Newman,[1] Jessica N. Aguilar,[2] Steven Ahlen,[3] Brett H. Andrews,[1] David Brooks,[4] Axel de la Macorra,[5] Arjun Dey,[6] Sarah Eftekharzadeh,[7] Andreu Font-Ribera,[8] Satya Gontcho A Gontcho,[2] Anthony Kremin,[2] Stephanie Juneau,[6] Martin Landriau,[2] Aaron Meisner,[9] Ramon Miquel,[10,8] John Moustakas,[11] Alan Pearl,[1] Francisco Prada,[12] Gregory Tarlé,[13] Małgorzata Siudek,[14,15] Benjamin Alan Weaver,[9] Zhimin Zhou,[16] and Hu Zou[16]

[1] *Department of Physics and Astronomy and PITT PACC, University of Pittsburgh, Pittsburgh, PA 15260, USA*

[2] *Lawrence Berkeley National Laboratory, 1 Cyclotron Road, Berkeley, CA 94720, USA*

[3] *Boston University, 590 Commonwealth Avenue, Boston, MA 02215, USA*

[4] *Department of Physics & Astronomy, University College London, Gower Street, London, WC1E 6BT, UK*

[5] *Instituto de Física, Universidad Nacional Autónoma de México, Cd. de México C.P. 04510, México*

[6] *NSF's NOIRLab, 950 N. Cherry Avenue, Tucson, AZ 85719, USA*

[7] *SOFIA Science Center, NASA Ames Research Center, Moffett Field, CA 94035, USA*

[8] *Institut de Física d'Altes Energies (IFAE), The Barcelona Institute of Science and Technology, Campus UAB, 08193 Bellaterra Barcelona, Spain*

[9] *NSF's NOIRLab, 950 N. Cherry Ave., Tucson, AZ 85719, USA*

[10] *Institució Catalana de Recerca i Estudis Avançats, Passeig de Lluís Companys, 23, 08010 Barcelona, Spain*

[11] *Department of Physics and Astronomy, Siena College, 515 Loudon Road, Loudonville, NY 12211*

[12] *Instituto de Astrofísica de Andalucía (CSIC), Glorieta de la Astronomía, s/n, E-18008 Granada, Spain*

[13] *University of Michigan, Ann Arbor, MI 48109*

[14] *Institute of Space Sciences (ICE, CSIC), Campus UAB, Carrer de Magrans, 08193 Barcelona, Spain*

[15] *Institut de Física d'Altes Energies (IFAE), The Barcelona Institute of Science and Technology, 08193 Bellaterra (Barcelona), Spain*

[16] *National Astronomical Observatories, Chinese Academy of Sciences, A20 Datun Rd., Chaoyang District, Beijing, 100012, P.R. China*

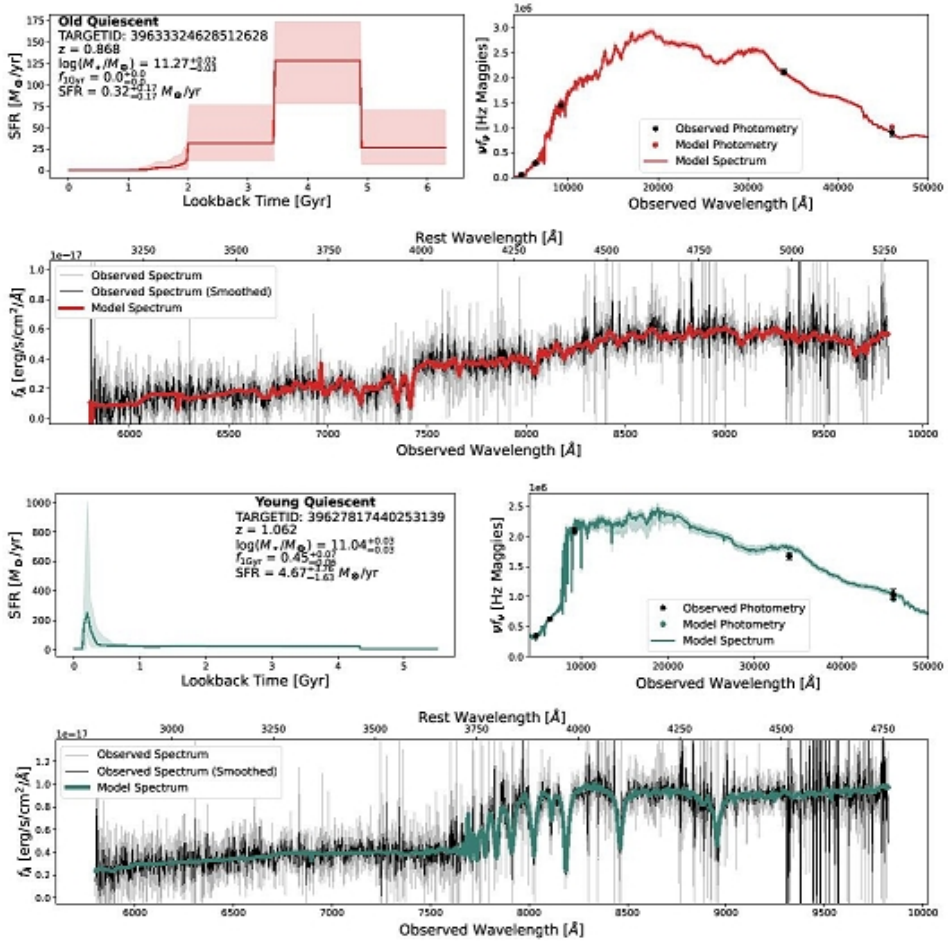

Figure 1. Example old (top, TARGETID=3963332462851262) and recently quenched (bottom, TARGETID=39627817440253139) galaxies from the DESI SV LRG Sample with `Prospector` fits using the star-formation history model from Suess et al. (2022a). For each galaxy, we show the median and 68% confidence interval star-formation history (top left) with selected galaxy properties. We also show the best fitting models (color) to the observed photometry ($g/r/z/W1/W2$, black) (top right). Finally, we show the DESI spectrum (observed, grey; 5 pixel boxcar smoothed, black) along with the best fitting model (color) (bottom). From this modeling, we identify quiescent LRGs and infer the dominance of recent star formation and the timescale of quenching.

Средняя экспозиция 2.4 часа

Отбор PSB из общего числа красных массивных галактик

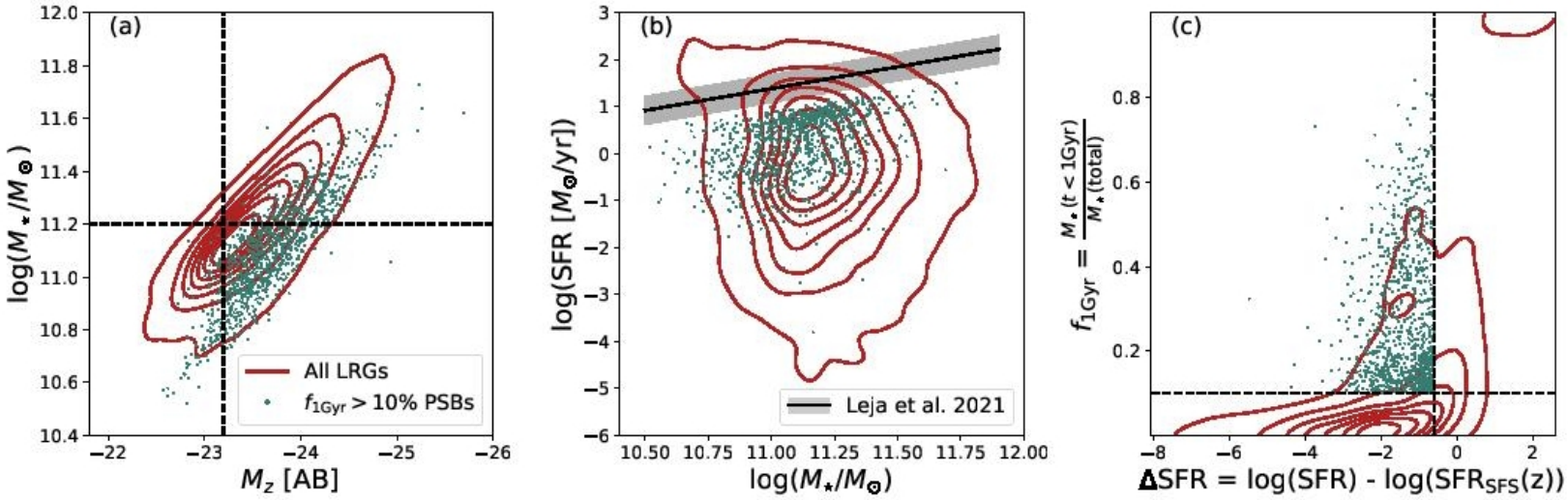

Figure 2. Properties of the full LRG sample (red contours) and a subset of post-starburst galaxies that recently quenched a significant episode of star formation using our fiducial selection ($f_{1Gyr} > 0.1$, $\Delta SFR < -0.6$, green points). All plotted points are the median values from the posterior of the `Prospector` fits. In panel (a), we show the stellar mass versus the absolute magnitude (M_z) along with the magnitude limited threshold ($M_z < -23.2$) and the mass complete threshold ($\log(M_\star/M_\odot > 11.2$) discussed in Section 2.3. In panel (b), we show the star-formation rate versus stellar mass, with the star-forming sequence at $z = 0.7$, the median redshift of our sample, shown as a black line with characteristic ~ 0.3 dex 1σ scatter (Leja et al. 2021). In panel (c), we show the post-starburst selection plane, f_{1Gyr} versus ΔSFR, with the fiducial selection cuts illustrated as dashed lines. The post-starburst sample is significantly brighter than the parent sample at fixed stellar mass and occupies a unique part of parameter space by having formed a significant amount of recent stellar mass despite being fully quenched.

Беспрецедентно много PSB на z>1; но это не volume-limited

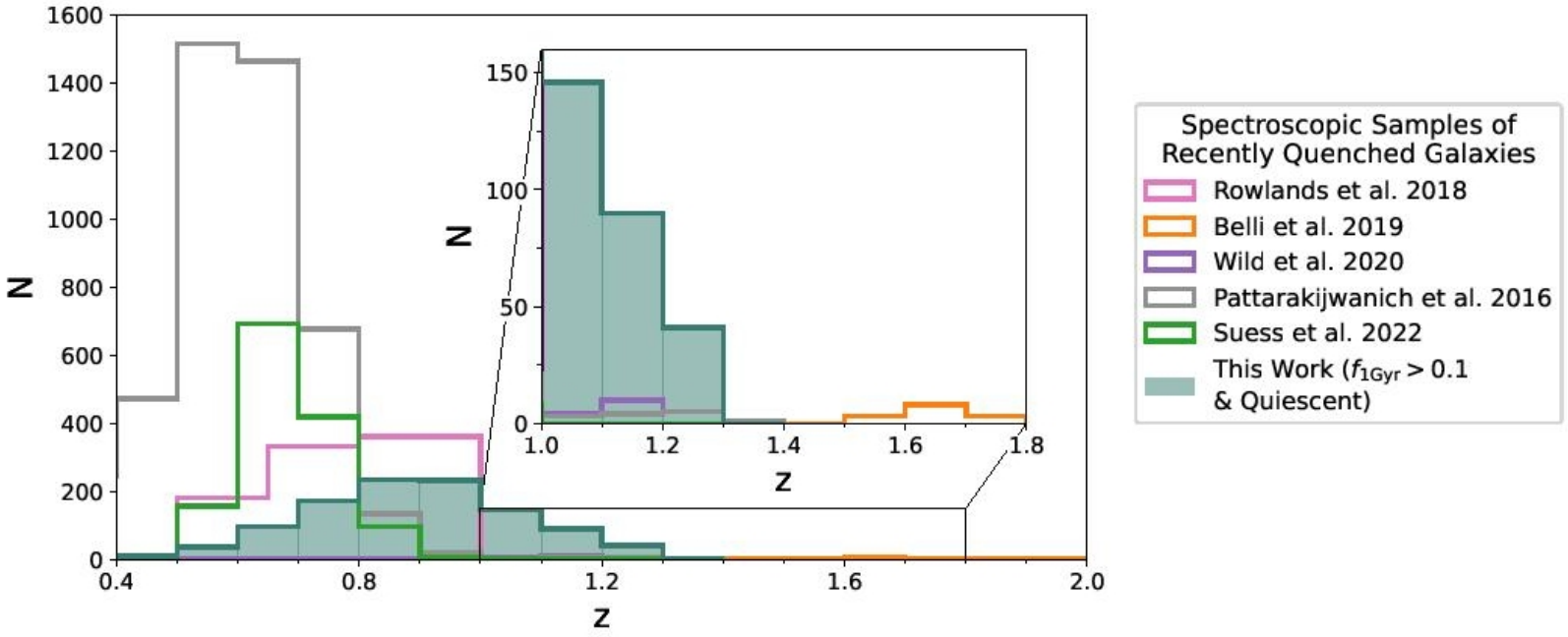

Figure 3. Redshift distributions of spectroscopic samples of recently quenched galaxies from $0.4 < z < 2.0$, with an inset focusing on $z > 1$ where the improvement in sample size from this work is most significant. Our fiducial post-starburst sample ($f_{1\mathrm{Gyr}} > 0.1$, $\Delta\mathrm{SFR} < -0.6$) is shown as a filled green histogram. Other samples shown include PCA-identified post-starburst galaxies from Rowlands et al. (2018) and Wild et al. (2020), galaxies with $t_{50} < 1.5$ Gyr from Belli et al. (2019), galaxies selected with K+A template fitting from the SDSS Pattarakijwanich et al. (2016), and galaxies selected using rest UBV filters from the SQuIGG$\vec{L}$E sample also selected from the SDSS (Suess et al. 2022b).

Эволюция числа (плотности) PSB

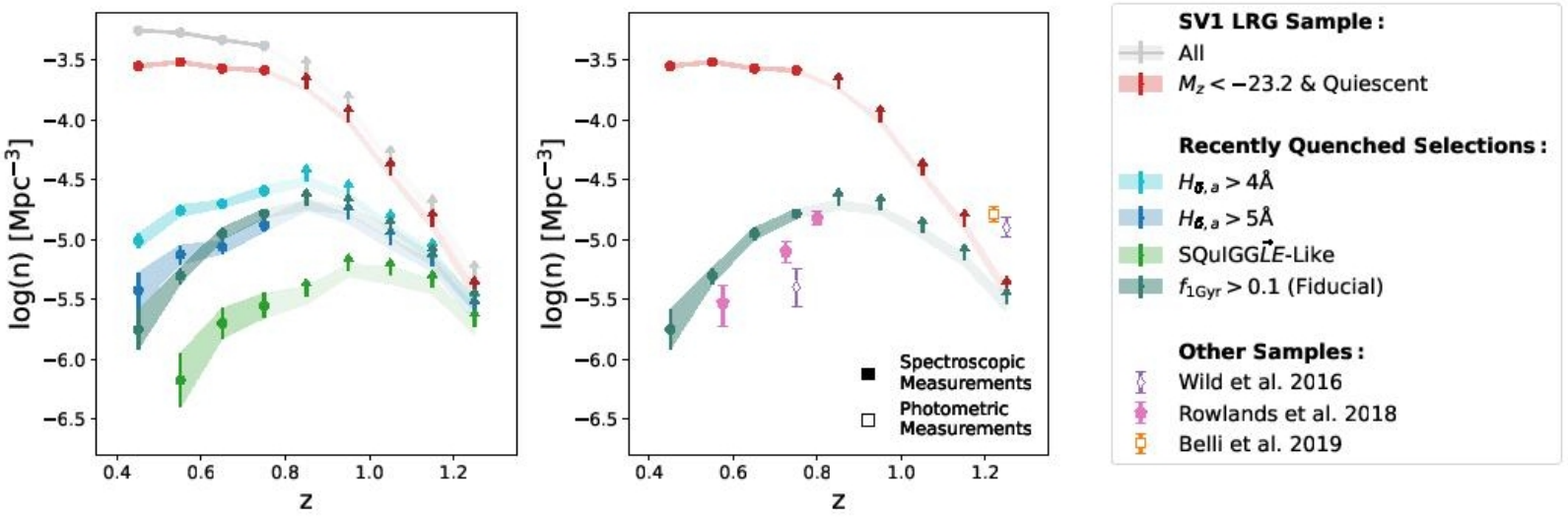

Figure 4. (Left): Number densities within the DESI SV LRG sample (full sample, gray; luminosity-complete and quiescent, red) and a variety of post-starburst selections from the luminosity-complete quiescent sample ($H_{\delta,a} > 4$, light blue; $H_{\delta,a} > 5$, dark blue; SQuIGG$\vec{L}$E SED selection, light green; and $f_{1\mathrm{Gyr}}$, green). Beyond $z \sim 0.8$, we indicate that the measured number densities are lower limits by plotting as upwared facing arrows. All post-starburst selections show an increasing number density over the redshift range in which we are complete, with varying normalization resulting from the relative restrictiveness of the post-starburst criteria. (Right): The same magnitude limited LRG and $f_{1\mathrm{Gyr}} > 0.1$ samples as the previous panel in addition to literature measurements (photometric: open symbols; spectroscopic: filled symbols). All three of the Wild et al. (2016) ($M_\star > 10^{10.8} M_\odot$), Rowlands et al. (2018) ($M_\star > 10^{11} M_\odot$), and Belli et al. (2019) ($M_\star > 10^{10.8} M_\odot$) samples show a trend of increasing number density with redshift, but the normalization differs between the different samples as a result of differing stellar mass limits and selection techniques.

Эволюция доли PSB

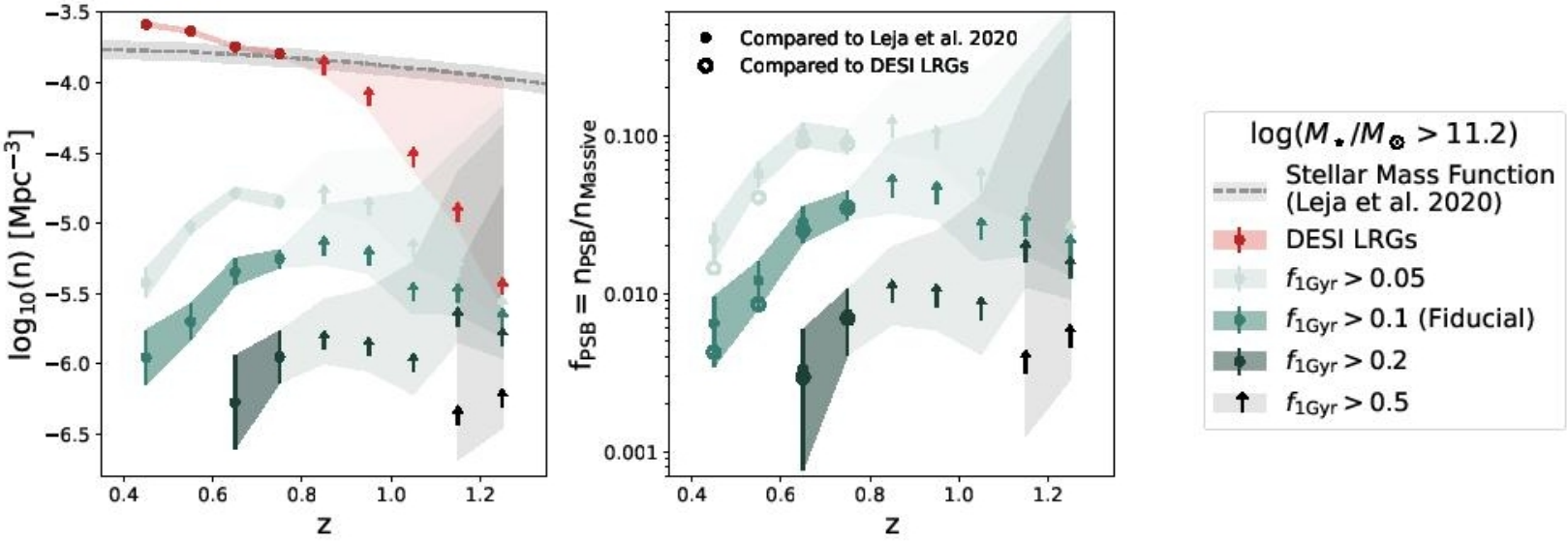

Figure 5. The number densities (left) and fractions (right) of recently quenched massive ($\log(M_\star/M_\odot) > 11.2$) galaxies. The dashed line and grey band (left) represent the stellar mass function of similarly mass galaxies (Leja et al. 2020), and the red points show the number density of all LRGs above the mass limit. The light green, green, dark green, and black points represent the number densities and fractions of recently quenched galaxies with $f_{1\mathrm{Gyr}}$ greater than 0.05, 0.1, 0.2, and 0.5 respectively, as compared to the stellar mass function from Leja et al. (2020). On the right panel, the open points of the same colors show the fraction of post-starburst galaxies as compared to our own massive galaxy number density measurements. Above $z = 0.8$, measurements are indicated as lower limits with errors inflated to encapsulate the possibility that all galaxies which were not targeted by DESI meet the selection criterion.

ArXiv: 2212.04480

Discovery and properties of the earliest galaxies with confirmed distances

[*1]Robertson, B. E., [*2,3]Tacchella, S., [4]Johnson, B. D., [5]Hainline, K., [5]Whitler, L., [4]Eisenstein D. J., [6]Endsley, R., [5]Rieke, M., [5]Stark, D. P., [5]Alberts, S., [7]Dressler, A., [5]Egami, E., [8]Hausen, R., [5]Rieke, G., [5]Shivaei, I., [9]Williams, C. C., [5]Willmer, C. N. A., [10]Arribas, S., [11,12]Bonaventura, N., [13]Bunker, A., [13]Cameron, A. J., [14]Carniani, S., [15]Charlot, S., [13]Chevallard, J., [2,3]Curti, M., [16]Curtis-Lake, E., [2,3]D'Eugenio, F., [11,12]Jakobsen, P., [2,3]Looser, T. J., [17]Lützgendorf, N., [2,3,18]Maiolino, R., [19]Maseda, M. V., [17]Rawle, T., [20]Rix, H.-W., [21]Smit, R., [2,3]Übler, H., [22]Willott, C., [2,3]Witstok, J., [23]Baum, S., [24]Bhatawdekar, R., [25,26]Boyett, K., [5]Chen, Z., [20]de Graaff, A., [5]Florian, M., [5]Helton, J. M., [5]Hviding, R. E., [5]Ji, Z., [27]Kumari, N., [5]Lyu, J., [28]Nelson, E., [2,3]Sandles, L., [13,18]Saxena, A.,[1,29]Suess, K. A., [5]Sun, F., [5]Topping, M. & [13]Wallace, I. E. B.

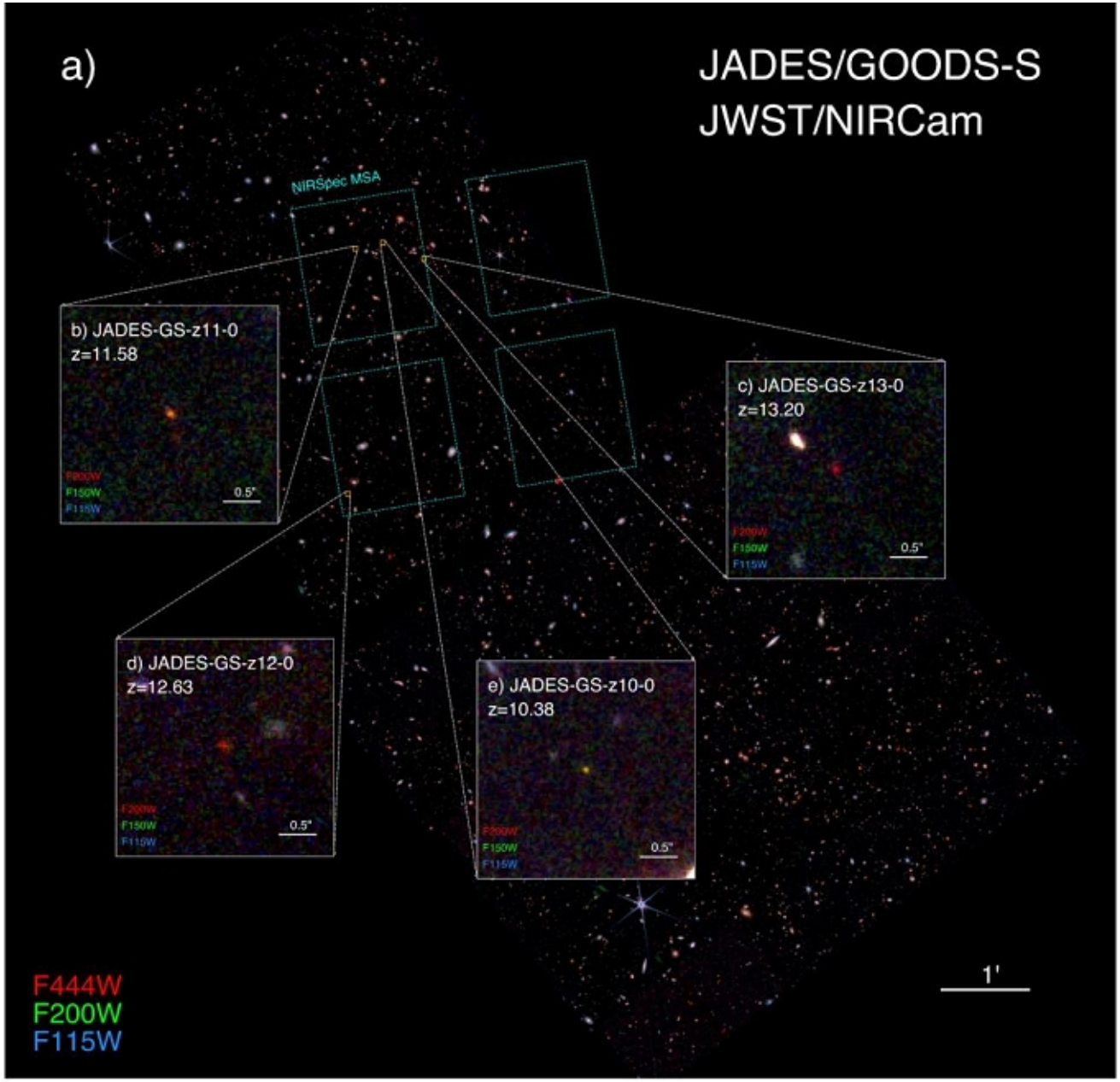

Fig. 1| Distant galaxies selected and confirmed by the JWST JADES program. From the JWST NIRCam imaging at wavelengths $\lambda \approx 0.8 - 5\ \mu m$ (F444W-F200W-F115W shown as a colour mosaic, **a**), galaxies with photometrically-determined redshift estimates of $z_{phot} > 10$ were selected for JWST NIRSpec MSA follow-up (footprint in cyan). An initial sample of four

Break-техника для далекой галактики

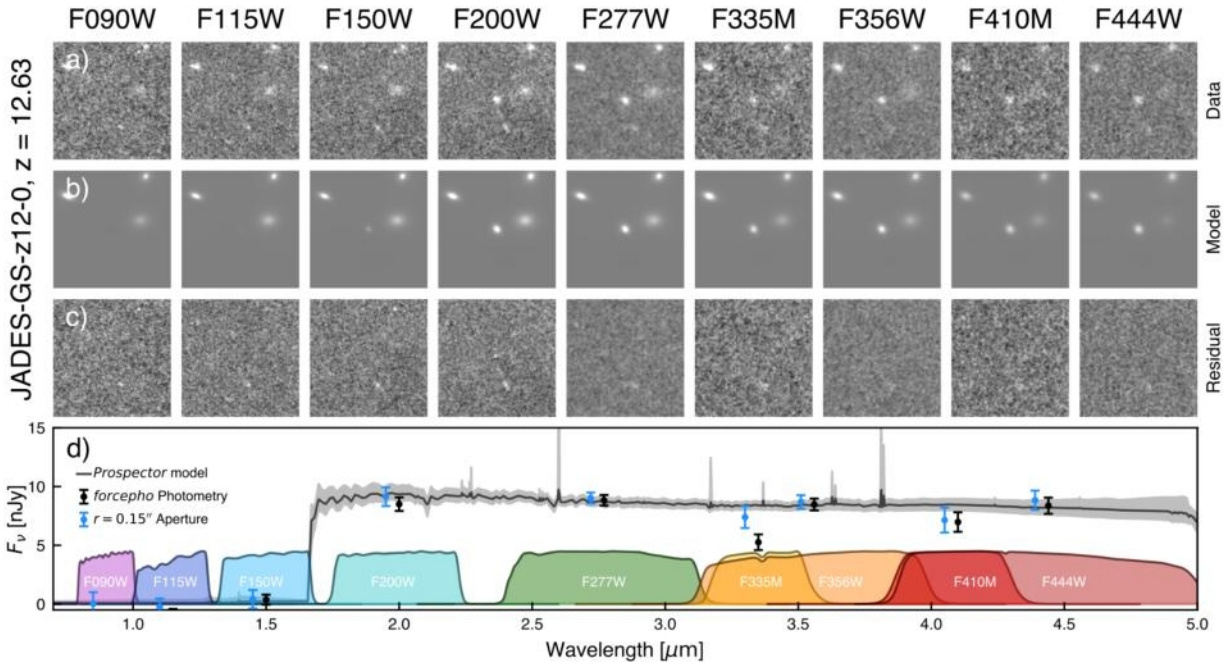

Fig. 2| Precision photometry and spectral energy distribution (SED) modelling of JADES-GS-z12-0. The sources detected by the JADES photometric pipeline are supplied to the *forcepho* scene modelling code, which then fits surface brightness profile models to the flux image of the object and its neighbours (**a**) in all NIRCam bands (columns, and filter curves in **d**) simultaneously. This method allows for the construction of accurate models of the observations (**b**) that leave only slight residuals (**c**) relative to the data. The source fluxes are then used as constraints for SED fitting (maximum likelihood fit, line in **d** with 1σ marginalised credibility

Параметры галактик – распределения вероятности

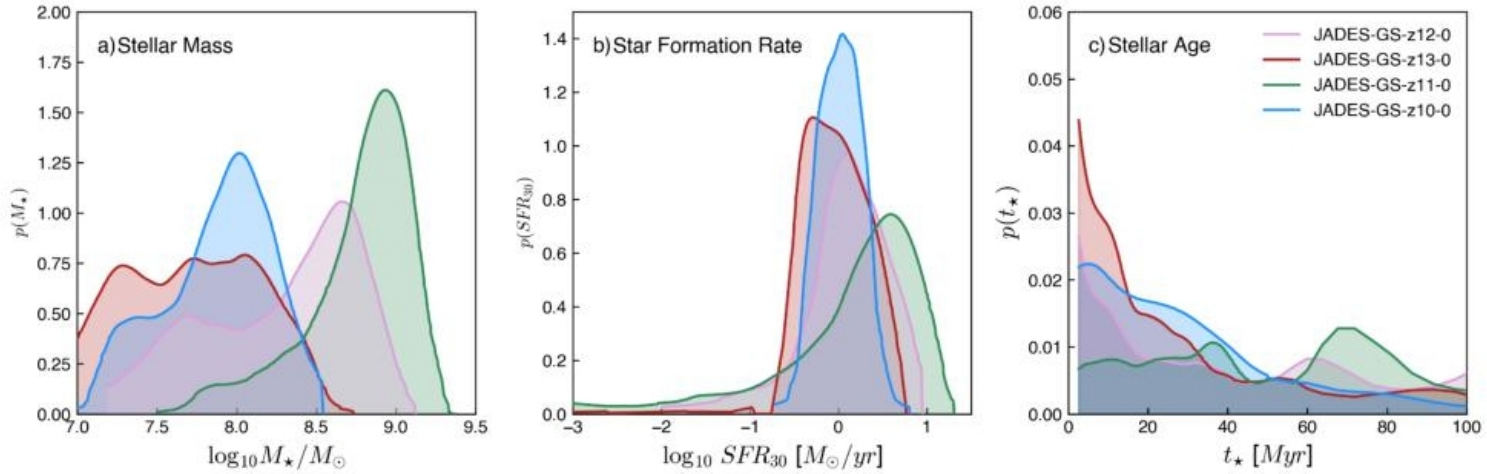

Fig. 3| Physical properties inferred from NIRCam imaging of distant, confirmed galaxies. Using population synthesis models that feature a flexible star formation history, possible nebular continuum and line emission, stellar evolutionary modelling, and the effects of dust, the observed NIRCam photometry and NIRSpec spectroscopic redshifts[10] are used to infer the stellar mass, star formation rate and history, and stellar age. Shown are the posterior distributions of the stellar mass (**a**), star formation rates (**b**), and mass-weighted median age of the stars (**c**) for the sample of z=10.4-13.2 galaxies presented here. We find a range of best-fit stellar masses of $log_{10}M_\star/M_\odot \sim 7.8-8.9$, star formation rates of $SFR \sim 1-2\ M_\odot/yr$, and ages of $t_\star \sim 16-71\ Myr$.

ArXiv: 2212.04568

Spectroscopy of four metal-poor galaxies beyond redshift ten

Emma Curtis-Lake[1*], Stefano Carniani[2†], Alex Cameron[3], Stephane Charlot[4], Peter Jakobsen[5,6], Roberto Maiolino[7,8,9], Andrew Bunker[3], Joris Witstok[7,8], Renske Smit[10], Jacopo Chevallard[3], Chris Willott[11], Pierre Ferruit[12], Santiago Arribas[13], Nina Bonaventura[5,6], Mirko Curti[7,8], Francesco D'Eugenio[7,8], Marijn Franx[14], Giovanna Giardino[15], Tobias J. Looser[7,8], Nora Lützgendorf[16], Michael V. Maseda[17], Tim Rawle[16], Hans-Walter Rix[18], Bruno Rodriguez del Pino[13], Hannah Übler[7,8], Marco Sirianni[16], Alan Dressler[19], Eiichi Egami[20], Daniel J. Eisenstein[21], Ryan Endsley[22], Kevin Hainline[20], Ryan Hausen[23], Benjamin D. Johnson[21], Marcia Rieke[20], Brant Robertson[24], Irene Shivaei[20], Daniel P. Stark[20], Sandro Tacchella[7,8], Christina C. Williams[25], Christopher N. A. Willmer[20], Rachana Bhatawdekar[26], Rebecca Bowler[27], Kristan Boyett[28,29], Zuyi Chen[20], Anna de Graaff[18], Jakob M. Helton[20], Raphael E. Hviding[20], Gareth C. Jones[3], Nimisha Kumari[30], Jianwei Lyu[20], Erica Nelson[31], Michele Perna[18], Lester Sandles[7,8], Aayush Saxena[3,9], Katherine A. Suess[24,32], Fengwu Sun[20], Michael W. Topping[20], Imaan E. B. Wallace[3] and Lily Whitler[20]

Первый спектральный обзор JWST

We specifically focus here on a pointing in the Hubble Ultra Deep Field (in the GOODS-South area), in which we have taken multi-object spectroscopy of 253 galaxies observed simultaneously with NIRSpec's configurable array of microshutters. We report here on observations taken with the prism spectral configuration (spectral range 0.6-5.3μm, resolving power R $\sim$ 100) with exposure times ranging from 9.3 to 28 hours (see Methods for details on the observing strategy).

The JADES spectroscopic observations reach an unprecedented sensitivity of 28.4 magnitudes (AB) at 5σ per resolution element on the continuum at 2.5μm. We note that the NIRSpec prism is extremely well-suited for the redshift confirmation of high-z candidates, with low spectral resolution and high sensitivity at short wavelengths where we are searching for a spectral break (around 1-2μm), and higher resolution in the 3-5 μm region, where we are searching for narrow spectral lines.

The focus of this paper is on four of these spectroscopic targets. Two of these are $z > 12$ galaxy candidates selected from NIRCam imaging [10], based on a clear lack of F150W flux. Two others are $z > 10$ candidates based on their *HST* IR photometry. We defer to description of the other targets in this deep pointing to a future publication. All candidates are faint, with F200W magnitudes fainter than 28 (AB), and hence entirely out of reach for any spectroscopic facility before *JWST*. More details on the selection and photometric

Вот эти спектры

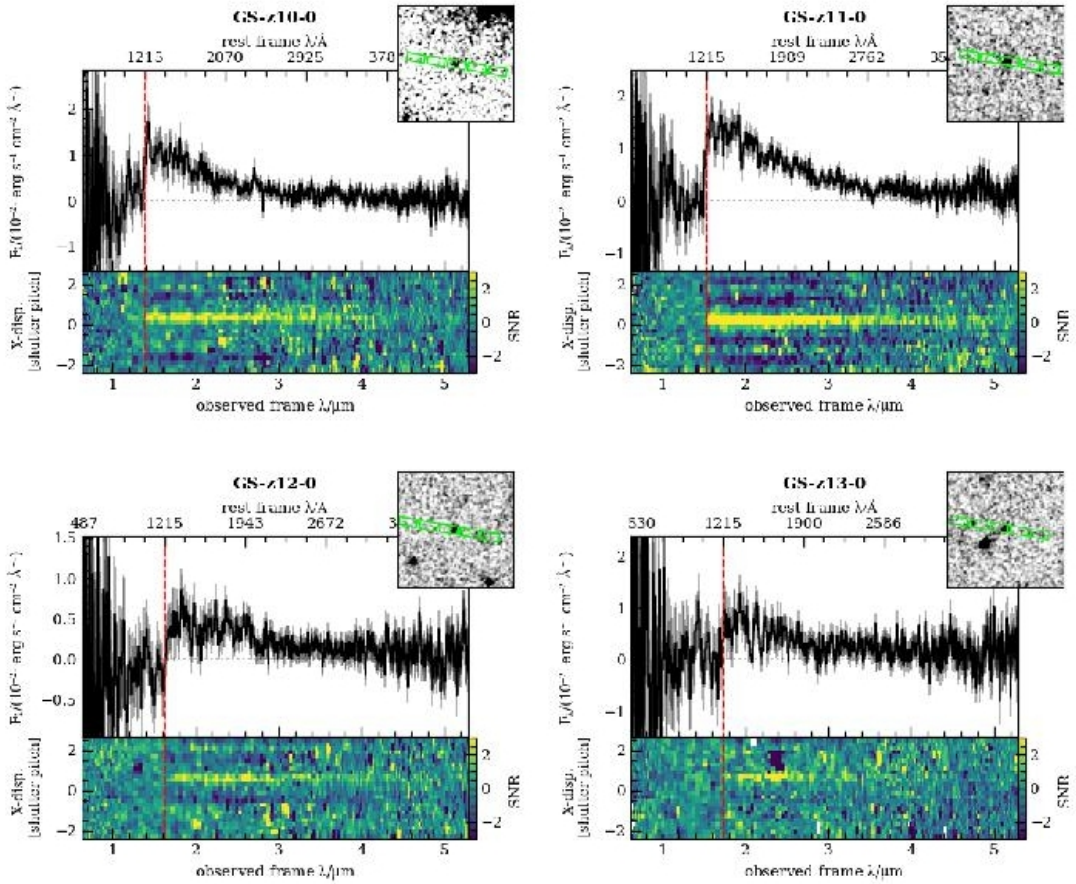

Fig. 1 NIRSpec prism $R \sim 100$ spectra for the four $z > 10$ galaxies targeted for the first deep spectroscopic pointing of the JADES survey, JADES-GS-z10-0, JADES-GS-z11-0, JADES-GS-z12-0 and JADES-GS-z13-0. For each galaxy we display the 1D spectrum and associated uncertainties. In the bottom panel we show the 2D signal-to-noise ratio plot. The 2D plot is binned over four pixels in the wavelength direction to better show the contrast across the break. The inset panel in the top right-hand corner shows the NIRCam F444W filter image with the three nodding positions of the the NIRSpec micro-shutter 3-slitlet array aperture shown in green. The red dashed line shows 1215.67Å at the observed redshift z_{1216}.

А вот параметры галактик, полученные по этим спектрам

Table 1 Exposure times, redshifts (derived both from assuming the spectral break is at exactly 1215.67Å and accounting for the damping wing from a fully neutral IGM), upper limits on emission line equivalent widths (rest frame) for the CIII]λ1907, 1909 and HeIIλ1640 lines, the 2σ lower limits on the strength of the observed spectral breaks (measurements described in Methods 2), UV absolute magnitude, M_{UV}, and UV-slope, β (measured directly from the spectra, see Methods 2.3) and BEAGLE-derived physical properties for the four objects. For the BEAGLE-derived properties we report posterior medians and limits in the 1σ credible region.

JADES-ID	GS-z10-0	GS-z11-0	GS-z12-0	GS-z13-0
Exposure time (s)	67225.6	100838.0	67225.6	33612.8
z_{1216}*	$10.38^{+0.07}_{-0.06}$	$11.58^{+0.05}_{-0.05}$	$12.63^{+0.24}_{-0.08}$	$13.20^{+0.04}_{-0.07}$
z_{HI}†	$10.37^{+0.03}_{-0.02}$	$11.48^{+0.03}_{-0.08}$	$12.60^{+0.04}_{-0.05}$	$13.17^{+0.16}_{-0.15}$
EW(CIII])/Å 2σ	< 13.8	< 5.9	< 12.4	< 15.2
EW(HeII)/Å 2σ	< 14.8	< 6.0	< 13.5	< 15.4
2σ break strength	> 2.04	> 6.85	> 2.48	> 2.79
M_{UV}	-18.61 ± 0.10	-19.34 ± 0.05	-18.23 ± 0.16	-18.73 ± 0.06‡
β	-2.49 ± 0.22	-2.18 ± 0.09	-1.84 ± 0.19	-2.37 ± 0.12‡
$\log(M/M_\odot)$	$7.58^{+0.19}_{-0.20}$	$8.67^{+0.08}_{-0.13}$	$7.64^{+0.66}_{-0.39}$	$7.95^{+0.19}_{-0.29}$
$\Psi/M_\odot\ yr^{-1}$¶	$1.1^{+0.19}_{-0.16}$	$2.2^{+0.28}_{-0.22}$	$1.8^{+0.54}_{-0.43}$	$1.36^{+0.31}_{-0.23}$
$\log(t/yr)$|	$7.54^{+0.25}_{-0.24}$	$8.35^{+0.08}_{-0.17}$	$7.36^{+0.75}_{-0.59}$	$7.84^{+0.23}_{-0.36}$
$\log(Z/Z_\odot)$**	$-1.91^{+0.25}_{-0.20}$	$-1.87^{+0.28}_{-0.18}$	$-1.44^{+0.23}_{-0.22}$	$-1.69^{+0.28}_{-0.31}$
$\hat{\tau}_V$††	$0.05^{+0.03}_{-0.02}$	$0.18^{+0.06}_{-0.06}$	$0.17^{+0.20}_{-0.09}$	$0.10^{+0.08}_{-0.05}$
ξ_{ion}§	$25.46^{+0.07}_{-0.07}$	$25.43^{+0.06}_{-0.06}$	$25.72^{+0.16}_{-0.19}$	$25.47^{+0.10}_{-0.09}$

*The redshift based on the spectral break being at 1215.67Å †The redshift accounting for a fully neutral IGM ($x_{HI} = 1$) following the method outlined in Methods 2.1. ‡For JADES-GS-z13-0, we report β and M_{UV} derived from the BEAGLE fitting, since we know this object to be on the edge of the shutter, and hence incorporate NIRCam photometry in the fitting to this one object to account for slit-losses (see Methods 3). ¶Ψ is the star formation rate. |t is age of the oldest stars, or maximum stellar age. **$\mathbf{Z}$ is the metallicity. ††$\hat{\tau}_V$ is the effective V-band attenuation optical depth. §The production rate of H-ionizing photons per unit monochromatic UV luminosity.